Peertechz

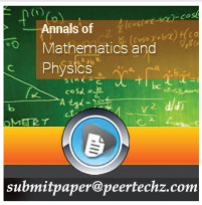

MATHEMATICS AND PHYSICS GROUP

ANNALS OF Mathematics and Physics OPEN ACCESS JOURNAL

ISSN: 2689-7636 DOI: https://dx.doi.org/10.17352/amp

Review Article

Analysis and Modeling of Heat and Mass Transfer in Alumina-water Nanofluids using Levenberg-Marquardt Backpropagation Neural Networks (LMT-ABPNN)

Imran Abbas*

Department of Mathematics, Air University, PAF Complex, Islamabad 44000, Pakistan

Received: 22 March, 2025
Accepted: 08 April, 2025
Published: 09 April, 2025

***Corresponding author:** Imran Abbas, Department of Mathematics, Air University, PAF Complex, Islamabad 44000, Pakistan, E-mail: imranabbasattari@gmail.com

Keywords: Artificial Backpropagation Neural Networks (ABPNN); Magnetohydrodynamics (MHD); Nanofluids; Levenberg-marquardt algorithm; Heat transfer modeling

https://www.mathematicsgroup.us

Check for updates

Abstract

This work examines the utilisation of artificial intelligence, particularly soft computing and machine learning, to augment robustness, enhance modelling precision, and facilitate swift assessment in nanofluid-based heat transfer systems. This research utilizes the Levenberg-Marquardt algorithm alongside Artificial Backpropagation Neural Networks to assess the efficacy of nanoparticles in convective heat transfer mechanisms.

The emphasis is on creating a comparison between Al_2O_3-H_2O nanoparticles and γ-Al_2O_3 in diverse base fluids, such as ethylene glycol and water, across an extensive surface area.The boundary layer flow is analysed under the effects of magnetohydrodynamics (MHD), incorporating slip boundary conditions and γ-Al_2O_3 nanofluids. This research examines a subject that has not been before investigated. The viscosity and thermal conductivity models for γ-Al_2O_3 nanofluids are established using empirical data, whereas thermal radiation effects are included into the Brinkman viscosity and Maxwell thermal conductivity models for Al_2O_3 nanofluids.The governing partial differential equations of magnetohydrodynamics are converted into ordinary differential equations using a suitable transformation. The dataset for the LMT-ABPNN model is produced using the Shooting method, which alters physical parameters across several situations, functioning as benchmarks for model training, validation, and testing. The efficacy of the LMT-ABPNN is assessed using measures like Mean Squared Error (MSE), error histograms, and regression analysis. The research examines the impact of many parameters on temperature, concentration, and velocity profiles. The Mean Squared Error (MSE) of the LMT-ABPNN model is assessed for several configurations of the Local Nusselt number in the Al_2O_3 -water system, with the Modified Local Nusselt number yielding the most precise prediction. The Sherwood number is employed to evaluate the model's efficacy in forecasting the power generation of waste heat recovery systems. The model has significant adaptability, with its gradient and learning rate underscoring its efficacy. The error histogram reveals negligible mistakes, suggesting possible avenues for additional optimization. The regression analysis of the alumina-water combination is illustrated in four graphs, which not only exhibit the model's present effectiveness but also highlight its potential for further enhancement.

1. Introduction

Traditional heat transfer fluids, like mineral oils and water, have limited thermal conductivity, adversely impacting industries such as chemical processing and transportation. Nonetheless, efficiency may be enhanced by the use of solid particle suspensions and fluids. Particles can be categorised in several manners, including distinctions based on metallic, non-metallic, and polymeric constituents. However, the widespread adoption of suspensions across several enterprises poses a series of challenges. These studies encompass the examination of factors such as the impact of erosion on thermal conductivity and the obstruction of flow pathways due to inadequate suspension stability. Furthermore, there is a gradual and persistent decline in pressure that intensifies these issues [1-3]. Researchers' efforts encompass the dispersion of particles at the millimetre or micrometre scale inside liquid media, a technique initially presented by Maxwell in 1873. The rapid sedimentation of larger particles in fluid systems is a significant challenge. Consequently, there is a growing focus on innovations designed to stimulate interest in nanotechnology heat transfer fluids, also known as "nanofluids." [4-8]. Nano fluids are utilized to evaluate the accuracy of engineering assertions and offer several

Citation: Abbas I. Analysis and Modeling of Heat and Mass Transfer in Alumina-water Nanofluids using Levenberg-Marquardt Backpropagation Neural Networks (LMT-ABPNN). Ann Math Phys. 2025;8(2):060-070. Available from: https://dx.doi.org/10.17352/amp.000147

advantages compared to conventional suspensions. These advantages encompass improved stability, augmented thermal conductivity, and diminished pressure loss. The examination of flow and heat transfer over a stretched sheet is a vital phenomenon with considerable ramifications for numerous industrial applications, where the effective regulation of heat and fluid flow is crucial for enhancing performance and energy efficiency [9-12]. These settings encompass several processes, including the cooling of metallic sheets, the facilitation of crystal growth in cooling solutions, the manufacture of plastic and rubber sheets, the creation of paper and glass fibres, and the enhancement of polymer and metal removal. In 1873, Maxwell first introduced the idea of improving thermal and electrical conductivity by the use of metallic particles. However, Choi's work done in the 1980s demonstrated that the use of conventional particles in micro-channel flow routes was impractical [13-15]. Recent research endeavours have investigated the behaviour of nanofluids in boundary layer flows across stretched surfaces. This research has examined a variety of nanoparticles composed of various metals and oxides. This work examines an enhanced version of Buongiorno's model and presents explicit thermo-physical correlations to assess the impact of Darcy-Forchheimer and Lorentz forces on the efficiency of alumina and water nanofluid flows that produce radiation. The study investigates the flow dynamics occurring across a curved, polished surface, constrained by various convective limitations [16-18]. Samia, et al. [19] employed the finite volume methodology to investigate the motion of micropolar nanofluids within a lid-driven cavity. Moreover, progress has been made in the creation of novel hybrid films that combine 2D and 3D graphene oxide with diamond microcomposites included in polyimide. This innovation seeks to enhance the conductivity of electrical and thermal energy. The exceptional thermal conductivity of this advanced technology renders it an excellent option for dissipating heat in the electrical components of electric machines [20]. Sabir, et al. [21] conducted a numerical investigation of the flow characteristics of a two-dimensional Sutterby fluid. The fluid was restricted to the vicinity of a spot exhibiting no flow and was subjected to an angled magnetic field and thermal radiation. Concurrently, Rehman, et al. [22] conducted an alternative computational analysis on the behaviour of a pseudo-plastic nanofluid near a flexible Riga sheet situated at a stagnation point. Ramesh, et al. [23] investigated the behaviour of an incompressible non-Newtonian fluid in stagnation-point flow across a non-isothermal stretching sheet.

Baag and colleagues, as cited in [24] developed numerical techniques to investigate the flow characteristics of magnetohydrodynamics. Polarisable fluids directed towards a stagnation point on a vertical surface. Efficient cooling rates are essential for industrial applications, including the cooling of metal sheets, crystal formation, and manufacturing processes. The quality of the output depends on the issues related to flow and heat transfer from stretched surfaces. Recent studies have mostly investigated the behaviour of nanofluids within the boundary layer over stretched surfaces. Nonetheless, there has been little research regarding the specific case of gamma alumina nanofluids [25-31]. Artificial Neural Networks (ANN) are powerful artificial intelligence systems that utilise several processors to assess and process data. These technologies are utilised in several fields such as bioinformatics, systems control, and temporal data forecasting. They enable activities including pattern recognition, regression analysis, modelling, and mapping. Artificial neural networks (ANNs) facilitate the minimisation of costs and time related to laboratory trials. Backpropagation, developed by Paul Werbos in 1974, minimises network error by gradient descent, whereas the Levenberg-Marquardt algorithm guarantees convergence and stability of artificial neural networks in fluid dynamics issues. Khan, et al. [32] used the Levenberg-Marquardt technique with an artificial backpropagated neural network (LMT-ABPNN) to investigate the heat transfer of nanoliquid flow between two parallel plates, considering Brownian and thermophoretic influences. Aljohani and associates [33] created a wire coating model employing LMT-ABPNN to replicate the behaviour of Eyring Powell liquid under diverse situations. Shah, et al. [34] have successfully modelled the flow of cross magneto nanoliquid under the influence of a magnetic force and a permeable cylindrical structure utilising LMT-ABPNN.

Novelty of the work

This paper presents an innovative methodology that combines the Levenberg-Marquardt Technique (LMT) with Artificial Backpropagation Neural Networks (ABPNN) to examine Magneto hydrodynamic (MHD) Stagnation Point Flow. This unique methodology, in contrast to standard methods, considers the dynamic interactions among stagnation point flow, concentration profiles, and the influence of magnetic fields, utilizing ethylene glycol and water as base fluids. This approach's distinctive feature is the synergistic integration of various components to develop a more precise and comprehensive model of MHD flows. Additionally, the study utilizes the shooting method to produce datasets for the training, validation, and testing stages, guaranteeing precise approximations of system dynamics. This work significantly contributes by a comprehensive investigation of flow behaviors, velocity profiles, concentration distributions, and temperature variations under diverse situations. Essential factors are altered to investigate the intricate connections among these variables—an element frequently overlooked in conventional models. This facilitates a comprehensive understanding of the system by concurrently evaluating many impacting aspects. The model's robustness is evidenced by accuracy assessments, error histograms, and regression analysis, establishing a strong basis for verifying the LMT-ABPNN technique. This distinguishes it from current models regarding reliability and performance. This work's originality lies in its capacity to manage nonlinear dynamics and accurately forecast complicated behavior patterns, establishing it as an essential instrument for future MHD research. The use of LMT-ABPNN in this scenario signifies a groundbreaking advancement, with no analogous investigation in the existing literature, so setting a new standard for future research.

The Levenberg-Marquardt Technique integrated with Artificial Backpropagation Neural Networks (LMT-ABPNN) is employed to estimate heat transfer in alumina-water Nano

Citation: Abbas I. Analysis and Modeling of Heat and Mass Transfer in Alumina-water Nanofluids using Levenberg-Marquardt Backpropagation Neural Networks (LMT-ABPNN). Ann Math Phys. 2025;8(2):060-070. Available from: https://dx.doi.org/10.17352/amp.000147

fluids. This innovative amalgamation of approaches provides deep insights into the complex dynamics of Nano fluid flows influenced by magneto hydrodynamics, representing a notable advancement in the area.

2. Mathematical modeling

Examine a theoretical situation with a two-dimensional laminar boundary layer characterized by incompressible flow. This flow presumes uniform physical qualities and entails the movement of water and ethylene glycol Nano fluids along an extended surface. The principal fluids examined in this context are water and ethylene glycol ($C_2H_6O_2$). The flow of Nano fluids is generated by sheet stretching along the x-axis, affected by two forces of similar size but differing directions. The stretching velocity indicates that the flow is restricted to the area where y is positive. The exterior velocity of the boundary layer flow is typically denoted as, which may be properly articulated as, where a constant value is indicated.

$$\tilde{u}_x + \tilde{v}_y = 0, \tag{1}$$

$$\tilde{u}\tilde{u}_x + \tilde{v}\tilde{u}_y = \frac{\mu_{nf}}{\rho_{nf}}\frac{\partial^2\tilde{u}}{\partial y^2} + \tilde{U}_\infty\frac{\partial\tilde{U}_\infty}{\partial x} - \frac{\sigma_{nf}B_0^2}{\rho_{nf}}(\tilde{u} - U_\infty) \tag{2}$$

$$\tilde{u}\tilde{T}_x + \tilde{v}\tilde{T}_y = \frac{k_{nf}}{(\rho C_p)_{nf}}\frac{\partial^2\tilde{T}}{\partial y^2} - \frac{1}{\tilde{\rho}\tilde{C}_p}\frac{\partial\tilde{q}_r}{\partial y} \tag{3}$$

$$\tilde{u}\tilde{C}_x + \tilde{v}\tilde{C}_y = D_{nf}\frac{\partial^2\tilde{C}}{\partial y^2} - k_1(C_1 - C\infty) \tag{4}$$

Radiative heat flux is estimated using the Rosseland approximation. utilizing variables such as $\tilde{u}$ and $\tilde{v}$, which denote the x and y velocity components, respectively, and $\tilde{\rho}$, which signifies fluid density. Furthermore, C_p denotes the specific heat at constant pressure.

$$\tilde{q}_r = -\left(\frac{4\tilde{\sigma}}{3\tilde{k}}\right)\frac{\partial T^4}{\partial y} \tag{5}$$

$$\left.\begin{aligned}\tilde{u} = u_w + L\frac{\partial u}{\partial y}, \tilde{v} = 0, \tilde{T} = T_w(T_w = T_\infty + bx^2), C = C_w = C_\infty + bx^2aty = 0,\\ \tilde{u} \to 0, \tilde{C} \to C_\infty, \tilde{T} \to T_\infty asy \to \infty\end{aligned}\right\} \tag{6}$$

Now introducing the stretching velocity U_∞ is given by $U_\infty(x) = ax$ where a is constant. Equation (1) is true by that the stream function is given by

$$\tilde{v} = \frac{\partial\psi}{\partial x}, \tilde{u} = \frac{\partial\psi}{\partial y} \tag{7}$$

3. Thermo physical properties

The thermo-physical parameters, particularly the heat capacity of Nano fluids, substantially affect their thermal performance. These nanoparticles, dispersed in a base fluid, alter their thermal conductivity, specific heat capacity, and viscosity, influencing their capability to store thermal energy and manage temperature variations. This variable substantially influences heat transfer rates and system efficiency.

$$\left.\begin{aligned}\rho_{nf} = (1-\varphi)\rho_f + \varphi\rho_s,\\ (\rho C_p)_{nf} = (1-\varphi)(\rho C_p)_f + \varphi(\rho C_p)_s\end{aligned}\right\} \tag{8}$$

The dynamic viscosity of Nano fluids can be expressed as

$$\left.\begin{aligned}\frac{\mu_{nf}}{\mu_f} = (1-\varphi)^{-2.5}(forAllAL_2O_3 - water)\\ \frac{\mu_{nf}}{\mu_f} = 123\varphi^2 + 7.3\varphi + 1(for\gamma - AL_2O_3 - water);\\ \frac{\mu_{nf}}{\mu_f} = 306\varphi^2 - 0.19\varphi + 1(for\gamma - AL_2O_3 - C_2H_6O_2)\end{aligned}\right\} \tag{9}$$

$$\left.\begin{aligned}\frac{k_{nf}}{k_f} = \frac{k_s + 2k_f - 2\varphi(k_f - k_s)}{k_s + 2k_f + \varphi(k_f - k_s)}(forAL_2O_3 - water)\\ \frac{k_{nf}}{k_f} = 4.97\varphi^2 + 2.72\varphi + 1(for\gamma - AL_2O_3 - water);\\ \frac{k_{nf}}{k_f} = 28.905\varphi^2 + 2.87\varphi + 1(for\gamma - AL_2O_3 - C_2H_6O_2)\end{aligned}\right\} \tag{10}$$

4. Similarity transformation

The similarity transformation, as delineated in Equation (11), is frequently utilized in the analysis of boundary layer flow issues. This transformation enables flow variables, including velocity, temperature, and concentration, to be articulated in terms of dimensionless variables, thus streamlining the analysis and diminishing its complexity. This transformation converts the governing partial differential equations (PDEs) into ordinary differential equations (ODEs), making them more amenable to solution. Within this paradigm, the subsequent relations are derived:

$$\left.\begin{aligned}\eta = \sqrt{\frac{a}{\nu_f}}y, \tilde{u} = axg'(\eta),\\ \tilde{v} = -(a\nu_f)^{\frac{1}{2}}g(\eta), \theta = \frac{\tilde{T} - T_\infty}{T_w - T_\infty}\varphi = \frac{\tilde{C} - C_\infty}{C_w - C_\infty}\end{aligned}\right\} \tag{11}$$

5. Momentum equation

$$\left.\begin{aligned}g''' - (1-\varphi)^{-2.5}\left(1-\varphi\left(\frac{\rho_s}{\rho_f}\right)\right)(g'-gg'') + \varepsilon^2 - M^2\frac{\sigma_{nf}}{\sigma_f}(g'-1) = 0 forAllAL_2O_3 - H_2O\\ g''' - \left(\frac{1-\varphi\left(\frac{\rho_s}{\rho_f}\right)}{306\varphi^2 - 0.19\varphi + 1}\right)(g'-gg'') + \varepsilon^2 - M^2\frac{\sigma_{nf}}{\sigma_f}(g'-1) = 0(for\gamma - AL_2O_3 - water);\\ g''' - \left(\frac{1-\varphi\left(\frac{\rho_s}{\rho_f}\right)}{123\varphi^2 + 7.3\varphi + 1}\right)(g'-gg'') + \varepsilon^2 - M^2\frac{\sigma_{nf}}{\sigma_f}(g'-1) = 0(for\gamma - AL_2O_3 - C_2H_6O_2)\end{aligned}\right\} \tag{12}$$

Citation: Abbas I. Analysis and Modeling of Heat and Mass Transfer in Alumina-water Nanofluids using Levenberg-Marquardt Backpropagation Neural Networks (LMT-ABPNN). Ann Math Phys. 2025;8(2):060-070. Available from: https://dx.doi.org/10.17352/amp.000147

6. Energy equation

$$\left.\begin{array}{c}\theta''\left(\frac{\tilde{k}_{nf}}{\tilde{k}_f}+\frac{4}{3}R\right)=p_r\left((1-\varphi)^{2.5}+\varphi\left(\frac{(\rho C_p)_s}{(\rho C_p)_f}\right)\right)(g\theta'-2\theta g') \\ for AL_2O_3-H_2O, \\ \theta''\left(\frac{\tilde{k}_{nf}}{\tilde{k}_f}+\frac{4}{3}R\right)=p_r\left((1-\varphi)^{2.5}+\varphi\left(\frac{(\rho C_p)_s}{(\rho C_p)_f}\right)\right)(g\theta'-2\theta g') \\ for \gamma-AL_2O_3-water \\ \theta''\left(\frac{\tilde{k}_{nf}}{\tilde{k}_f}+\frac{4}{3}R\right)=p_r\left((1-\varphi)^{2.5}+\varphi\left(\frac{(\rho C_p)_s}{(\rho C_p)_f}\right)\right)(g\theta'-2\theta g') \\ for \gamma-AL_2O_3-C_2H_6O_2\end{array}\right\} \quad (13)$$

7. Concentration equation

$$\left.\begin{array}{c}\varphi''+Sc(f\varphi'-2f'-\gamma_2\varphi)=0. \\ for AL_2O_3-H_2O,\end{array}\right\} \quad (14)$$

8. Boundary conditions

The boundary conditions that correspond to this are provided as.

$$\left.\begin{array}{c}g(0)=0,\varphi(0)=1,g'(0)=1 \text{ and } g'(\infty)=0, \\ \theta(0)=1 \text{ and } \theta(\infty)=0=\varphi(\infty).\end{array}\right\} \quad (15)$$

9. Critical engineering parameters for analysis

The skin friction coefficient and the Nussle number are essential physical parameters in the analysis of fluid dynamics and heat transfer across various systems. The skin friction coefficient measures the shear stress imposed by the fluid on the surface, serving as a critical indicator of flow resistance. Conversely, the Nussle number is a dimensionless quantity that delineates the ratio of convective to conductive heat transfer in fluid flow. Both parameters are indispensable for comprehending and enhancing heat transfer rates, especially in industrial applications involving Nano fluids. The interaction between these parameters can profoundly influence thermal efficiency and frictional losses in systems such as heat exchangers, internal combustion engines, and fluid transport systems. The skin friction coefficient and the Nusselt number are the significant physical interest parameters for the problem. C_f is given as

$$c_f=-\frac{-2\mu_{nf}}{\rho_f u_w^2}(u_y)_{y=0} \quad (16)$$

Using equation 12 skin friction can be written as

$$\left.\begin{array}{c}\frac{1}{2}Re_x^{\frac{1}{2}}c_f=-(1-\varphi)^{-2.5}g''(0) \\ for All AL_2O_3-H_2O \\ \frac{1}{2}Re_x^{\frac{1}{2}}c_f=-(123\varphi^2+7.3\varphi+1)g''(0), \\ for \gamma-AL_2O_3-H_2O \\ \frac{1}{2}Re_x^{\frac{1}{2}}c_f=-(306\varphi^2-0.19\varphi+1)g''(0) \\ for \gamma-AL_2O_3-C_2H_6O_2\end{array}\right\} \quad (17)$$

The Nussle number is defined as

$$Nu_x=\frac{x\tilde{q}_w}{\tilde{k}_f(T_w-T_\infty)} \quad (18)$$

$$\tilde{k}_{nf}(T_y)_{y=0}=\tilde{q}_w \quad (19)$$

The Sherwood number is expressed as:

$$Sh_x=\frac{x\tilde{q}_m}{\tilde{D}_{nf}(C_w-C_\infty)} \quad (20)$$

$$\tilde{D}_{nf}(C_y)_{y=0}=\tilde{q}_m \quad (21)$$

$$\left.\begin{array}{c}Re_x^{\frac{1}{2}}Nu_x=\left(\frac{k_s+2k_f-2\varphi(k_f-k_s)}{k_s+2k_f+\varphi(k_f-k_s)}\right)(-\theta'(0)) \\ for AL_2O_3-H_2O) \\ Re_x^{-\frac{1}{2}}Nu_x=(4.97\varphi^2+2.72\varphi+1)(-\theta'(0)) \\ for \gamma-AL_2O_3-H_2O \\ \frac{k_{nf}}{k_f}=(28.905\varphi^2+2.87\varphi+1)(-\theta'(0)) \\ for \gamma-AL_2O_3-C_2H_6O_2\end{array}\right\} \quad (22)$$

Table 1 presents the results of the LMT-ABPNN model for the local Nussle number (N. number), skin friction coefficient (S. friction), and Sherwood number (Sh. number) using alumina-water Nano fluids.

The Table 1 displays the results of the Levenberg-Marquardt method utilizing Artificial Backpropagation Neural Networks (LMT-ABPNN) for three principal physical parameters: the local Nusselt number (φ_1), skin friction coefficient (φ_2), and Sherwood number (φ_3), pertaining to alumina-water (Al_2O_3-H_2O) nanofluids. The table presents Mean Squared Error (MSE) values for training, validation, and testing, showing a substantial decrease from training to testing, which signifies effective model generalization. The performance measure, indicative of the model's overall efficiency, is shown for each

Table 1: Results of LMT-ABPNN for local Nusselt number ϕ_1(N.number), ϕ_2 skin friction coe_cient (S.friction), and ϕ_3 Sherwood number (Sh.number) with nanoparticle ϕ_1 (Al_2O_3 = H_2O).

Phys.	MSE	Training	Validation	Testing	Performance	Grad
φ_1	1.30×10^{-8}	3.24×10^{-9}	1.20×10^{-10}	1.31×10^{-6}	1.89×10^{-5}	1.00×10^{-8}
φ_2	$5.77.30\times10^{-11}$	4.45×10^{-9}	6.09×10^{-10}	2.99×10^{-9}	1.08×10^{-8}	1.00×10^{-7}
φ_3	2.66×10^{-7}	3.40×10^{-8}	2.60×10^{-8}	2.64×10^{-7}	1.94×10^{-5}	1.00×10^{-7}

Citation: Abbas I. Analysis and Modeling of Heat and Mass Transfer in Alumina-water Nanofluids using Levenberg-Marquardt Backpropagation Neural Networks (LMT-ABPNN). Ann Math Phys. 2025;8(2):060-070. Available from: https://dx.doi.org/10.17352/amp.000147

quantity, displaying values from 1.31×10^{-6} to 2.64×10^{-7}. The gradient (Grad) values, essential for model optimization, together with the μ (Mu) values for each physical quantity, are also included. The results validate the LMT-ABPNN's capacity to precisely forecast the heat and mass transport characteristics of nanofluids, affirming the model's efficacy throughout several training phases.

Numerical results

Code validation: Table 2 presents a complete comparison of the values of -f''(0) for the Al_2O_3-water combination. This evaluation is predicated on the findings delineated independently by Hamad, et al. [14], Vishnu, et al. [35], and Abbas, et al. [36]. The consistency with prior findings supports the validity of the current computational approach. The graphic images reinforce this consensus by visually representing the previously provided facts. The authors investigate the impact of nanoparticle volume fraction on several characteristics, including velocity and temperature profiles, skin friction coefficient, and reduced Nusselt number, utilizing visual aids.

Table 2: Comparison of Results.

φ	Hamid [14]	Vishnu, et al. [35]	Abbas, et al. [36]	Present work
0.05	1.00538	1.00537	1.00530	1.00530
0.10	0.99877	0.99877	0.98866	0.98867
0.15	0.98185	0.98184	0.97132	0.97131
0.20	0.95992	0.95991	0.94581	0.94580

Variation in parameters influences the local Nusselt numbers, skin friction, and Sherwood numbers through ANN

The Figure 1(a) displays the Mean Squared Error (MSE) depiction of LMT-ABPNN, which is based on several variations of the Local Nussle number for the Al_2O_3-water system. Its formula is:

$$MSE = (1/n) * \Sigma (ypredi - ytruei)^2$$

The findings indicate that the LMT-ABPNN model, incorporating the Modified Local Nussle number, has the lowest Mean Squared Error (MSE). The findings suggest that the Modified Local Nussle number is the most accurate parameter for predicting the Local Nussle number using the LMT-ABPNN model.

The graph 2(a) displays the average standard error (MSE) representation of the LMT-ABPNN model, considering several modifications of the skin friction coefficient number. The Mean Squared Error (MSE) quantifies the discrepancy between the expected and actual values of the skin friction coefficient. A smaller mean squared error (MSE) signifies superior predictive ability of the model in estimating the skin friction coefficient value. The graph indicates that the LMT-ABPNN model, when using the original skin friction coefficient number, has the lowest Mean Squared Error (MSE). These findings suggest that the initial skin friction coefficient value is the most accurate parameter for forecasting the skin friction coefficient value.

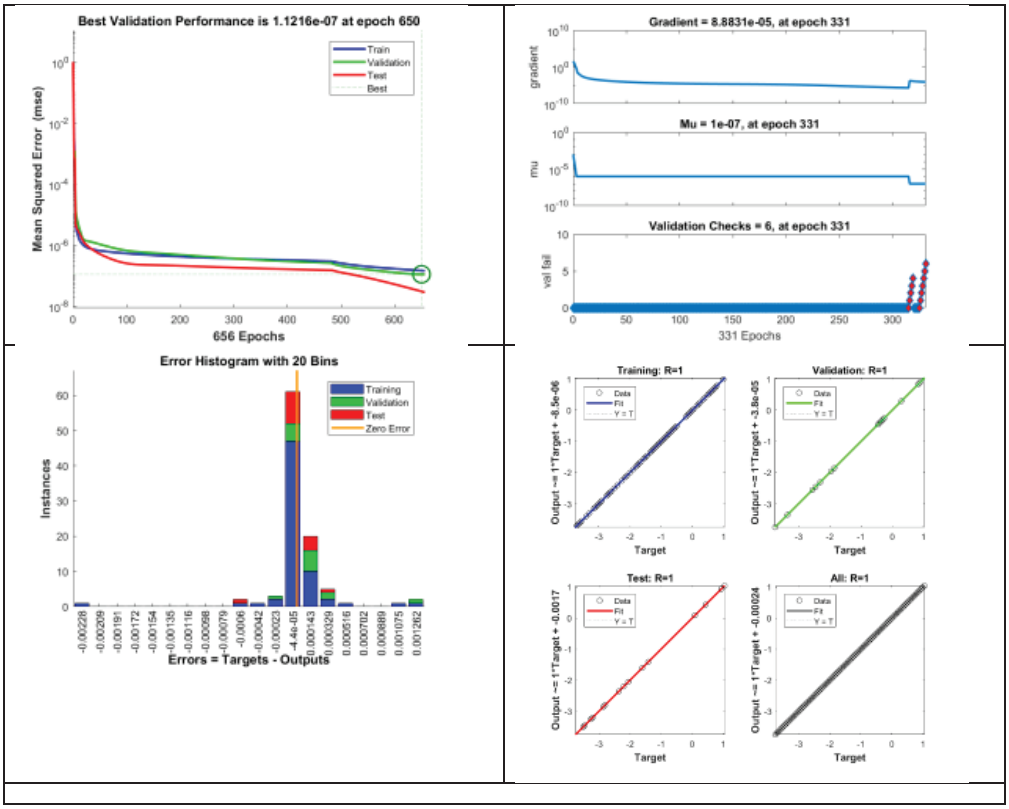

Figure 1: Graphical illustration of LMT-ABPNN based on several variations of Local Nussle number for the Al_2O_3-water(a) MSE representation (b)Results of the transition state,(c) Histogram for error analysis (d) Regression.

Citation: Abbas I. Analysis and Modeling of Heat and Mass Transfer in Alumina-water Nanofluids using Levenberg-Marquardt Backpropagation Neural Networks (LMT-ABPNN). Ann Math Phys. 2025;8(2):060-070. Available from: https://dx.doi.org/10.17352/amp.000147

The figure above discusses the LMT-ABPNN model. The alternative forms of the skin friction coefficient, including the modified, normalized, and logarithmically transformed versions, exhibit worse performance compared to the original skin friction coefficient. This implies that these deviations are less successful in capturing the intricate correlations between the input and output variables of the LMT-ABPNN model.

The Sherwood number 3 (a) is a useful metric for assessing the efficacy of a deep learning model in forecasting the power generation of a waste heat recovery system. A greater Sherwood number signifies the model's enhanced ability to accurately represent the intricate connections between the input and output variables. Nevertheless, it is crucial to acknowledge that the Sherwood number alone represents a single measure of model performance. Additional criteria, such as the precision and resilience of the model, should also be taken into account. The graphic displays the gradient and learning rate for the era. The gradient quantifies the extent to which the weights of the model are adjusting in relation to the training data. A smaller gradient suggests that the model is approaching a solution. The learning rate is a parameter that governs the magnitude of the adjustments made to the weights of the model. An elevated learning rate can accelerate the model's learning process, but it can also result in overfitting. Reducing the learning rate will result in a slower learning process for the model, but it will decrease the likelihood of overfitting.

The graphs 2(b) indicate a decreasing gradient, a suitable reduction in mu, and a plateauing of the validation checks. These findings indicate that the deep learning model is acquiring knowledge efficiently and demonstrating strong adaptability to unfamiliar material. In summary, the graphic indicates that the deep learning model is undergoing efficient training and is prepared for deployment in a production environment.

The graph 3 (b) shows that the gradient is initially high, but it decreases over time as the model converges. Mu is also high at first, but it is gradually reduced to prevent the model from overfitting the training data. The validation checks initially increase, but they plateau towards the end of training. This suggests that the model is learning to generalize well to unseen data. Figure1(c) displays error histograms is a useful tool for evaluating the performance of the LMT-ABPNN model. The prevalence of minor errors implies that the model can effectively forecast the local Nussle number for the *Al*203–water system. Nevertheless, the existence of certain significant flaws indicates that the model is not flawless, and more enhancements can still be made. In summary, the error histogram demonstrates that the LMT-ABPNN model. The model successfully predicts the local Nussle number for the Al_2O_3-water system with high accuracy. Figure display 2(c) The error histogram, consisting of 20 bins, is constructed using many changes of the skin friction coefficient for the Al_2O_3-water system. It displays the frequency of mistakes taken in each bin. The error histogram indicates that the bulk of errors fall below 0.001, with a prominent peak occurring at about 0.0005. There exist a few mistakes over 0.001, however, they constitute a minority. The LMT-ABPNN model's performance

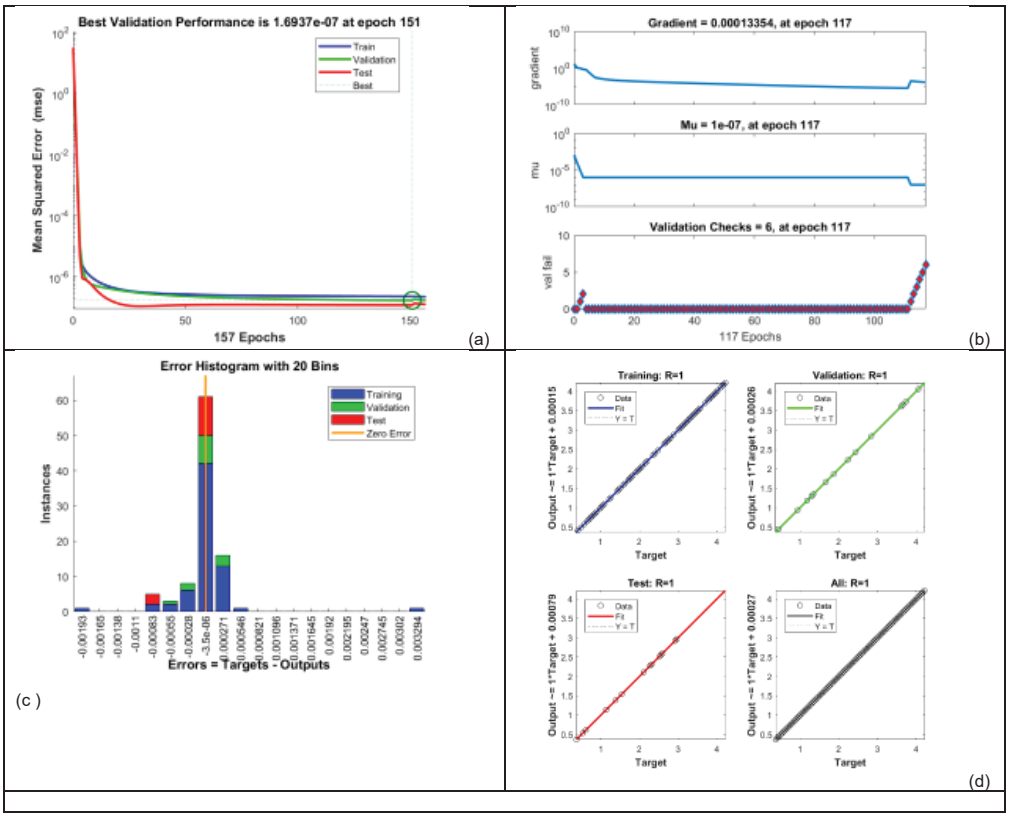

Figure 2: Graphical illustration of LMT-ABPNN based on several variations of Local Nussle number for the $$Al_2O_3$-water$(a) MSE representation (b)Results of the transition state,(c) Histogram for error analysis (d) Regression.

Citation: Abbas I. Analysis and Modeling of Heat and Mass Transfer in Alumina-water Nanofluids using Levenberg-Marquardt Backpropagation Neural Networks (LMT-ABPNN). Ann Math Phys. 2025;8(2):060-070. Available from: https://dx.doi.org/10.17352/amp.000147

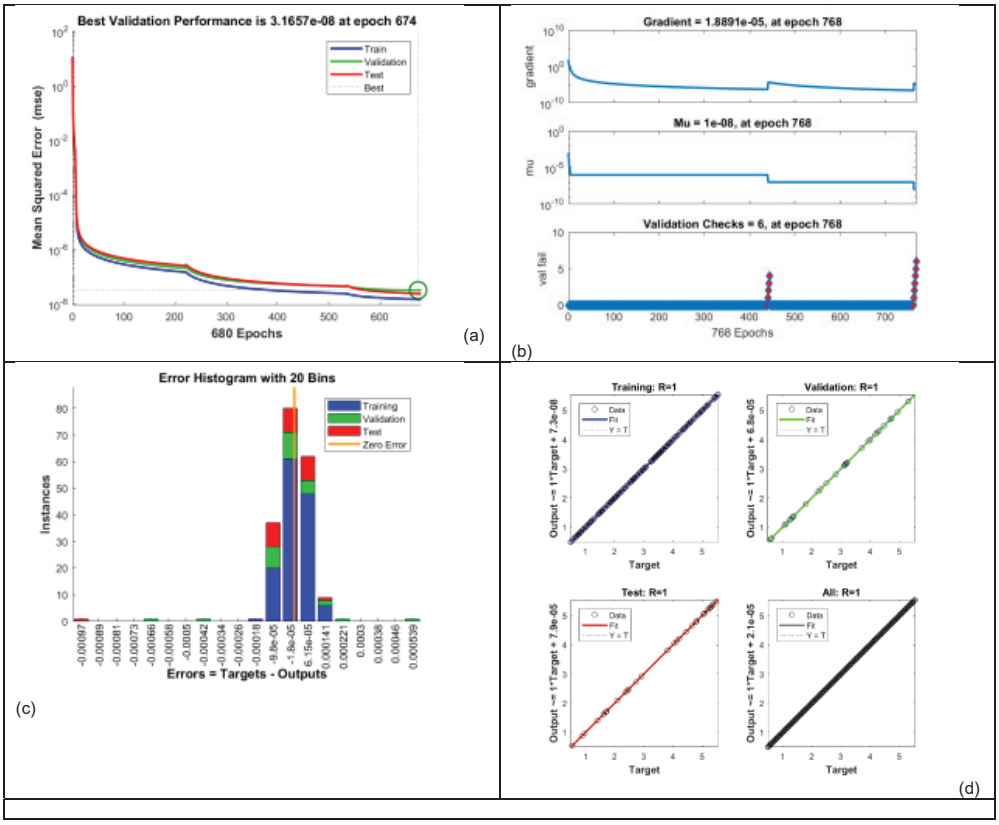

Figure 3: Graphical illustration of LMT-ABPNN based on several variations of Local showered number (a) MSE representation (b)Results of the transition state,(c) Histogram for error analysis (d) Regression.

can be evaluated using the error histogram. The model's small errors indicate accurate prediction of the Al_2O_3-water system's skin friction coefficient. However, larger errors suggest room for improvement. To enhance performance, more training data and a different neural network architecture could be used, as the LMT-ABPNN is simple.

Figure 3(c) the error histogram, based on 20 bins of Local Sherwood Number (LSN) variations, is a useful tool for error analysis in LMT-ABPNN. It helps identify common error magnitudes, compare the performance of different LSN variations, and analyze the error distribution. The histogram shows a skewed distribution, suggesting the LMT-ABPNN is overestimating outputs. The most common error magnitude is around 0.0004, indicating the LMT-ABPNN is predicting outputs within 0.4%.

Figure display1, 2, 3(d) regression task is shown four graphs depicting the performance of the LMT-ABPNN model on the Al_2O_3-water regression problem, utilizing different changes of the local Nussle number. The plots display the training, validation, and overall datasets, respectively. The LMT-ABPNN model exhibits strong concordance with the target data across all four graphs, as evidenced by a correlation coefficient (R) of 1 in each instance. This suggests that the model possesses a high capacity to comprehend the correlation between the input and output variables. Nevertheless, there exist nuanced variations in the model's performance across the various data sets. On the training and validation data sets, the slope of the LMT-ABPNN fit line is marginally lower than the slope of the target data line. This indicates that the model is inadequately fitting the training data to a certain degree. The slope of the LMT-ABPNN fit line is marginally greater than the slope of the target data line, as observed on the test and all data sets. This indicates that the model is excessively fitting the training data to a certain degree. Nevertheless, the disparity in gradient is minute, and the total correlation coefficient remains exceptionally high.

Effects of velocity and temperature profile: As shown in Figure 4 depicts the changes in velocity of different Nano fluids as the concentration of nanoparticles rises. The results suggest that there is a direct relationship between the amount of nanoparticles in oxide Nano fluids and the velocities in water.

Nano fluids composed of γ - Al_2O_3 exhibit enhanced fluid velocity due to the presence of a comparatively thicker momentum barrier layer. The momentum boundary layer refers to the fluid layer adjacent to a solid surface, wherein the fluid velocity is influenced by the presence of the surface. A larger momentum boundary layer facilitates enhanced fluid-particle interaction duration, resulting in enhanced velocity. Nano fluids comprising ethylene glycol exhibit enhanced fluidity compared to Nano fluids composed of water. The reason for this phenomenon is attributed to the increased viscosity of ethylene glycol in comparison to water, resulting in a slower flow of the fluid through a solid surface. This process results in an increase in the thickness of the outer layer of momentum, thereby leading to an increase in speed. The dissimilarity in

Citation: Abbas I. Analysis and Modeling of Heat and Mass Transfer in Alumina-water Nanofluids using Levenberg-Marquardt Backpropagation Neural Networks (LMT-ABPNN). Ann Math Phys. 2025;8(2):060-070. Available from: https://dx.doi.org/10.17352/amp.000147

momentum boundary layer thickness is evident, as water-based Nano fluids exhibit a narrower layer compared to ethylene glycol-based Nano fluids. The discrepancy in velocity is evident, as Al_2O_3 – water Nano fluids exhibit a lower velocity in comparison to $\gamma - Al_2O_3$ – ethylene glycol Nano fluids.

Figure 5 shows how nanoparticle volume fraction affects Nano fluid temperature profiles. Al_2O_3 and $\gamma - Al_2O_3$ Nano fluids, higher nanoparticle volume fractions improve temperatures. In comparison to base fluids, the temperature profile is elevated to a greater extent in Nano fluids based on water, whereas it is relatively lower in Nano fluids based on ethylene glycol. The reason for the difference stems from the fact that water exhibits a considerably lower Prandtl number in comparison to ethylene glycol, indicating that water possesses a better thermal diffusivity than ethylene glycol. After conducting a comparison of nanoparticles, it becomes apparent that the temperature profile of Al_2O_3 – water Nano fluids is higher in magnitude when compared to that of $\gamma - Al_2O_3$ – water Nano fluids. Nevertheless, when considering Nano fluids based on ethylene glycol, the temperature profile of $\gamma - Al_2O_3$ is shown to be higher compared to that of Al_2O_3.

The graphical representation depicted in Figure 6 illustrates the inclination of the velocity as influenced by variations in the stagnation parameter. As the value of the stagnation parameter increases, there is a corresponding increase in the velocity of the Nano fluids. Nevertheless, throughout this procedure, there is a rise in both temperature and nanoparticle volume fraction. When the stream velocity is held constant, an increase in the stagnation parameter value results in a decrease in the stretch velocity of the system. This statement suggests that there is an intricate relationship between the stagnation parameter, velocity, temperature, and nanoparticle volume fraction in the phenomena of Nano fluid flow.

Figure 7 illustrates the impact of radiation heat flux on the velocity profile of three distinct fluids: water, ethylene glycol, and Al_2O_3-water Nano fluid. The velocity profile is represented on the x-axis of the graph, while the radiative heat flow is represented on the y-axis. The graph displays three distinct curves, each representing a different fluid. The graph clearly demonstrates that the radiative heat flow rises in correlation with velocity for all three fluids. The Al_2O_3-water Nano fluid exhibits the maximum radiative heat flow, followed by ethylene

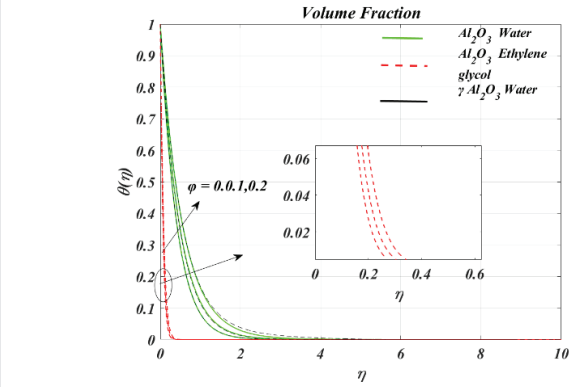

Figure 5: Variation of temperature profile with Nanoparticle Volume Fraction Φ.

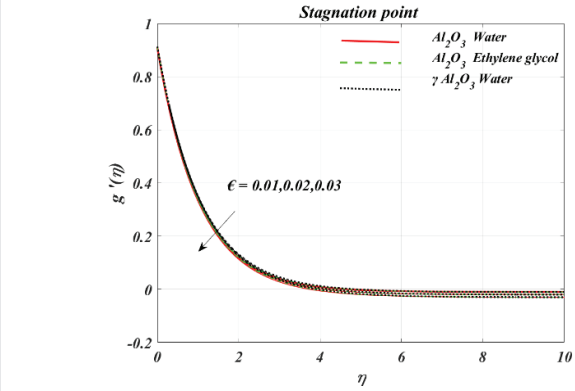

Figure 6: Stagnation points effect with velocity profile.

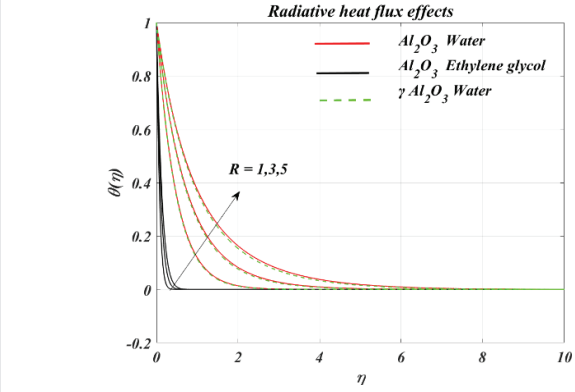

Figure 7: Impacts of Radiative Heat R Flux on velocity Profile.

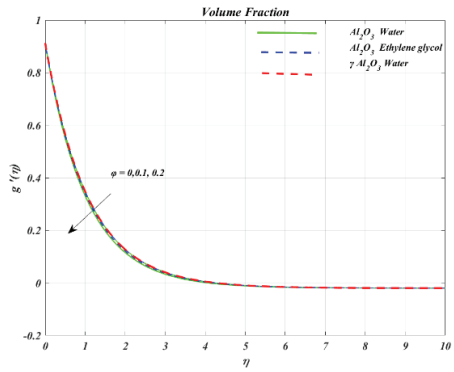

Figure 4: Variation of Velocity profile with Nanoparticle Volume Fraction Φ.

glycol and then water. The enhanced radiation absorption and scattering properties of the Nano fluid can be attributed to the presence of Al_2O_3 nanoparticles. The impact of radiative heat flow is especially significant at low velocities. At elevated speeds, the influence of convective heat transfer becomes increasingly prominent.

Figure 8 illustrates the results obtained by varying the radiative heat flux parameter, denoted as R. The temperature profile exhibits enhancement as the radiative heat flux increases, while conversely, the velocity profile experiences a decline. Although there is a slight decrease observed in the velocity profile for specific values of improved thermal

Citation: Abbas I. Analysis and Modeling of Heat and Mass Transfer in Alumina-water Nanofluids using Levenberg-Marquardt Backpropagation Neural Networks (LMT-ABPNN). Ann Math Phys. 2025;8(2):060-070. Available from: https://dx.doi.org/10.17352/amp.000147

radiation, there is also a slight increase noticed for another range of values. These outcomes indicate that manipulating the parameter R, which represents thermal radiation, has a negligible impact on fluid velocity. This holds true even though the velocity profile displays a minor declining tendency. Indeed, it is a fact that fluid viscosity tends to increase when faced with heightened resistance to distortion, leading to a decrease in the velocity profile. Conversely, there is a tendency for fluid viscosity to decrease as both internal heat production and thermal radiation experience an upsurge (Figure 9).

The findings about the temperature profile are depicted in the figures referred to as ref.9. It is clear that there is a connection between the slip parameter, which is denoted by the letter a, and the similarity variable, which is designated by the letter η, in terms of the velocity and temperature profiles. It is important to note that a decrease in the Nano fluid's velocity results from an increase in the slip velocity parameter. At the same time, an increase in the same parameter is equivalent to an increase in the temperature.

Figure 10 demonstrates a direct correlation between water's magnetic field and its velocity, wherein the magnetic strength heightens as velocity increases. This phenomenon stems from heightened water molecule polarization resulting from swifter motion, thereby generating a magnetic field. Furthermore, the the extent of polarization escalates in tandem with the concentration of Al_2O_3 in the water. This alignment is due to Al_2O_3's paramagnetic nature, indicating its affinity for magnetic fields. The graph further shows that the incline of the curve reduces as the concentration of Al_2O_3 grows. This outcome arises from the intensified polarization of water molecules in the presence of Al_2O_3, leading to a dampened increment in the magnetic field as velocity increases.

Variation in parameters influences the local Nusselt numbers, skin friction

The variations in the local skin friction coefficient and the compact Nussle number are depicted in figures referred to as ref. 11 and ref. 12, respectively. On the horizontal axis of both images is the representation of the nanoparticle volume percentage. On the vertical axis of images 8 and 9, respectively, is the presentation of the local skin friction coefficient and the lowered Nussle number. There is a clear correlation between

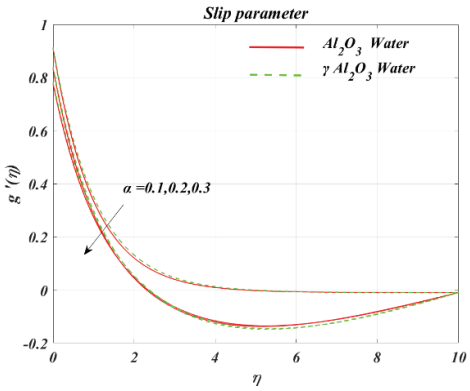

Figure 9: Influence of Slip Parameter$ on Velocity Profile.

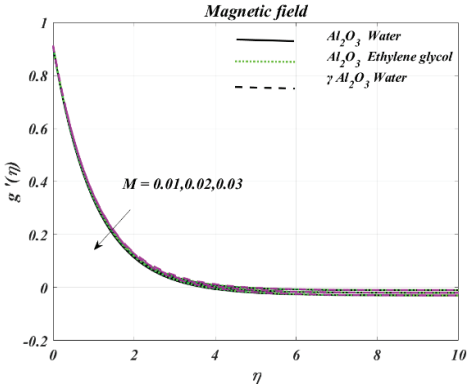

Figure 10: Impacts of Magnetic Field$ on Velocity Profile.

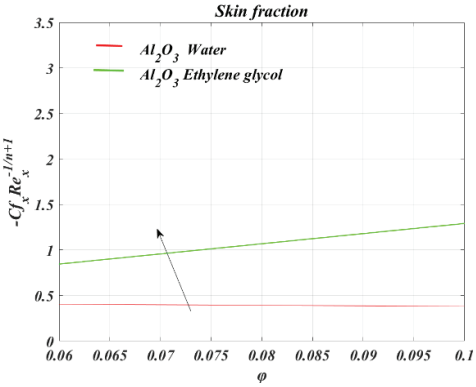

Figure 11: Frictional Efficiency of Skin as a Function of Φ.

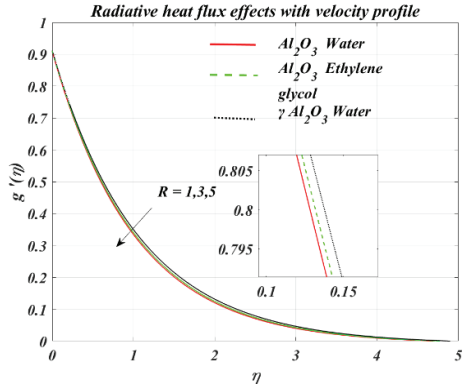

Figure 8: Impacts of Radiative Heat R Flux on velocity Profile.

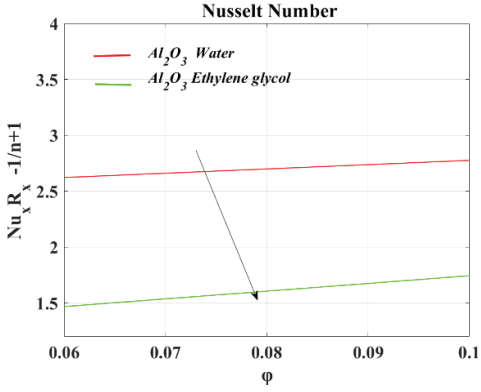

Figure 12: Frictional Efficiency of Nussle number as a Function of Φ.

Citation: Abbas I. Analysis and Modeling of Heat and Mass Transfer in Alumina-water Nanofluids using Levenberg-Marquardt Backpropagation Neural Networks (LMT-ABPNN). Ann Math Phys. 2025;8(2):060-070. Available from: https://dx.doi.org/10.17352/amp.000147

an increase in the phi values and a matching rise in the skin friction coefficient as well as the Nussle number. This was demonstrated. Therefore, the skin friction coefficient for $\gamma - Al2O3$ Nano fluid is somewhat larger than it is for $Al2O3$. When various base fluids are taken into consideration, the skin friction coefficient that results from Al_2O_3 with water as the base fluid has a higher value than the skin friction coefficient that results from Al_2O_3 with ethylene glycol as the base fluid.

On the other hand, it seems that the gamma – Al_2O_3 nanoparticles are following the opposite pattern. Notably, the Nussle numbers of Nano fluids that use ethylene glycol as their base fluid are significantly greater than those of Nano fluids that use water as their base fluid. In addition, as compared to the other nanoparticle options available, gamma – Al_2O_3 nanoparticles display noticeably elevated Nussle values.

10. Conclusion

This paper introduces a unique methodology for examining convective heat transport in nanofluids, with particular emphasis on comparing Al_2O_3-H_2O and γ-Al_2O_3 nanoparticles in diverse base fluids. We need to understand the complex system behind this phenomenon. under magnetohydrodynamic (MHD) circumstances by utilising the Levenberg-Marquardt algorithm and Artificial Backpropagation Neural Networks (LMT-ABPNN), therefore overcoming deficiencies in prior studies. The efficacy of the LMT-ABPNN model is evidenced by comprehensive assessment metrics, such as Mean Squared Error (MSE), error histograms, and regression analysis, validating its robust flexibility and accuracy in forecasting critical heat transfer parameters.The results underscore the precision of the Modified Local Nusselt number as an essential metric for assessing the thermal efficacy of the nanofluid system. Furthermore, the Sherwood number demonstrates efficacy in predicting the energy output of waste heat recovery systems. The low error rates seen in the model's predictions indicate considerable possibilities for enhancing the modelling of heat transfer in nanofluid-based systems. Future research may explore on enhancing these models, investigating other nanoparticle forms, and broadening their applicability to a wider range of industrial uses. The use of AI-driven methodologies like LMT-ABPNN in nanofluid heat transfer modelling facilitates effective thermal management solutions, with prospective applications in energy systems, electronic cooling, and industrial heat exchangers.

References

1. Das SK, Choi SU, Yu W, Pradeep T. Nanofluids: science and technology. Hoboken: John Wiley & Sons; 2007. 416 p. Available from: https://www.wiley.com/en-us/Nanofluids%3A+Science+and+Technology-p-9780470074732
2. Gupta J, Pandey BK, Dwivedi DK, Mishra S, Jaiswal RL. Three-level homogeneous model for the study of heat transfer mechanism in metallic nanofluids. Physica B Condens Matter. 2023;662:414973. Available from: https://doi.org/10.1016/j.physb.2023.414973
3. Choi SU, Eastman JA. Enhancing thermal conductivity of fluids with nanoparticles. Argonne (IL): Argonne National Lab.; 1995. Technical Report. Available from: https://www.researchgate.net/publication/236353373
4. Ramireddy SV, Janardhan K, Umamaheswar M, Reddy PC, Kumar VR. Flow characteristics of MHD radiative heat absorbing/generating nanofluid with variable temperature. [Journal info incomplete]
5. Guled CN, Tawade JV, Kumam P, Noeiaghdam S, Maharudrappa I, Chithra SM, et al. The heat transfer effects of MHD slip flow with suction and injection and radiation over a shrinking sheet by optimal homotopy analysis method. Results Eng. 2023;18:101173. Available from: https://doi.org/10.1016/j.rineng.2023.101173
6. Turkyilmazoglu M. Dual and triple solutions for MHD slip flow of non-Newtonian fluid over a shrinking surface. Comput Fluids. 2012;70:53–8. Available from: https://doi.org/10.1016/j.compfluid.2012.01.009
7. Sheikholeslami M, Abelman S, Ganji DD. Numerical simulation of MHD nanofluid flow and heat transfer considering viscous dissipation. Int J Heat Mass Transf. 2014;79:212–22. Available from: https://doi.org/10.1016/j.ijheatmasstransfer.2014.08.004
8. Sheikholeslami M, Abelman S. Two-phase simulation of nanofluid flow and heat transfer in an annulus in the presence of an axial magnetic field. IEEE Trans Nanotechnol. 2015;14(3):561–9. Available from: http://dx.doi.org/10.1109/TNANO.2015.2416318
9. Jamaludin A, Naganthran K, Nazar R, Pop I. Thermal radiation and MHD effects in the mixed convection flow of Fe3O4–water ferrofluid towards a nonlinearly moving surface. Processes. 2020;8(1):95. Available from: https://doi.org/10.3390/pr8010095
10. Farajollahi B, Etemad SG, Hojjat M. Heat transfer of nanofluids in a shell and tube heat exchanger. Int J Heat Mass Transf. 2010;53(1-3):12–7. Available from: https://doi.org/10.1016/j.ijheatmasstransfer.2009.10.019
11. Rehman R, Wahab HA, Khan U. Heat transfer analysis and entropy generation in the nanofluids composed by aluminum and γ-aluminum oxides nanoparticles. Case Stud Therm Eng. 2022;31:101812. Available from: https://doi.org/10.1016/j.csite.2022.101812
12. Ejaz A, Abbas I, Nawaz Y, Arif MS, Shatanawi W, Abbasi JN, et al. Thermal analysis of MHD non-Newtonian nanofluids over a porous media. CMES Comput Model Eng Sci. 2020;125(3):1119–34. Available from: https://doi.org/10.32604/cmes.2020.012091
13. Soltanipour H, Choupani P, Mirzaee I. Numerical analysis of heat transfer enhancement with the use of γ-Al2O3 water nanofluid and longitudinal ribs in a curved duct. Therm Sci. 2012;16(2):469–80. Available from: http://dx.doi.org/10.2298/TSCI110719028S
14. Hamad MAA. Analytical solution of natural convection flow of a nanofluid over a linearly stretching sheet in the presence of magnetic field. Int Commun Heat Mass Transf. 2011;38(4):487–92. Available from: https://doi.org/10.1016/j.icheatmasstransfer.2010.12.042
15. Arif MS, Jhangir M, Nawaz Y, Abbas I, Abodayeh K, Ejaz A, et al. Numerical study for magnetohydrodynamic (MHD) unsteady Maxwell nanofluid flow impinging on heated stretching sheet. CMES Comput Model Eng Sci. 2022;133(2):303–25. Available from: https://doi.org/10.32604/cmes.2022.020979
16. Algehyne EA, Wakif A, Rasool G, Saeed A, Ghouli Z. Significance of darcy-forchheimer and Lorentz forces on radiative alumina-water Nano fluid flows over a slippery curved geometry under multiple convective constraints: a renovated buongiorno's model with validated thermophysical correlations. Waves Random Complex Media. 2022:1–30. Available from: https://doi.org/10.1080/17455030.2022.2074570
17. Alrabaiah H, Iftikhar A, Saeed A, Bilal M, Eldin SM, Galal AM. Numerical calculation of darcy forchheimer radiative hybrid nanofluid flow across a curved slippery surface. S Afr J Chem Eng. 2023;45:172–181. Available from: https://doi.org/10.1016/j.sajce.2023.05.013

Citation: Abbas I. Analysis and Modeling of Heat and Mass Transfer in Alumina-water Nanofluids using Levenberg-Marquardt Backpropagation Neural Networks (LMT-ABPNN). Ann Math Phys. 2025;8(2):060-070. Available from: https://dx.doi.org/10.17352/amp.000147

18. Boonsatit N, Sohail M, Mukdasai K, Nazir U, Singh M, Singh A, et al. Galerkin computational work on thermally enhancement process in complex rheological generalized theory due to 3d-partially ionized rotational flow. Case Stud Therm Eng. 2023;42:102709. Available from: https://doi.org/10.1016/j.csite.2023.102709

19. Batool S, Rasool G, Alshammari N, Khan I, Kaneez H, Hamadneh N. Numerical analysis of heat and mass transfer in micro polar Nano fluids flow through lid driven cavity: Finite volume approach. Case Stud Therm Eng. 2022;37:102233. Available from: https://doi.org/10.1016/j.csite.2022.102233

20. Bhutta MS, Xuebang T, Akram S, Yi-dong C, Ren X, Fasehullah M, et al. Development of novel hybrid 2d-3d graphene oxide diamond micro composite polyimide films to ameliorate electrical & thermal conduction. Case Stud Therm Eng. 2022;37:102235. Available from:

21. Sabir Z, Imran A, Umar M, Zeb M, Shoaib M, Raja MAZ. A numerical approach for 2-d sutterby fluid-flow bounded at a stagnation point with an inclined magnetic field and thermal radiation impacts. Therm Sci. 2021;25(3 Part A):1975–1987. Available from: https://doi.org/10.2298/TSCI191207186S

22. Rehman A, Hussain A, Nadeem S. Assisting and opposing stagnation point pseudoplastic nano liquid flow towards a flexible riga sheet: A computational approach. Math Probl Eng. 2021:1–14. Available from: https://doi.org/10.1155/2021/6610332

23. Ramesh GK, Prasannakumara BC, Gireesha BJ, Rashidi MM. Case study on MHD micro polar fluid flow near the stagnation point over a stretching sheet with variable thickness and radiation. J Appl Fluid Mech. 2016;9(3):1115–1022.

24. Baag S, Mishra SR, Dash GC, Acharya MR. Numerical investigation on MHD micro polar fluid flow toward a stagnation point on a vertical surface with heat source and chemical reaction. J King Saud Univ Eng Sci. 2017;29(1):75–83. Available from: https://doi.org/10.1016/j.jksues.2014.06.002

25. Rashidi MM, Erfani E. The modified differential transform method for investigating Nano boundary-layers over stretching surfaces. Int J Numer Methods Heat Fluid Flow. 2011;21(7):864–883. Available from: https://www.emerald.com/insight/content/doi/10.1108/09615531111162837/full/html

26. Turkyilmazoglu M. Exact analytical solutions for heat and mass transfer of MHD slip flow in nanofluids. Chem Eng Sci. 2012;84:182–187. Available from: https://doi.org/10.1016/j.ces.2012.08.029

27. RamReddy C, Murthy PVSN, Chamkha AJ, Rashad AM. Soret effect on mixed convection flow in a Nano fluid under convective boundary condition. Int J Heat Mass Transf. 2013;64:384–392. Available from: https://doi.org/10.1016/j.ijheatmasstransfer.2013.04.032

28. Akbar NS, Nadeem S, Ul Haq R, Khan ZH. Radiation effects on MHD stagnation point flow of Nano fluid towards stretching surface with convective boundary condition. Chin J Aeronaut. 2013;26(6):1389–1397. Available from: https://doi.org/10.1016/j.cja.2013.10.008

29. Rashidi MM, Momoniat E, Ferdows M, Basiriparsa A. Lie group solution for free convective flow of a Nano fluid past a chemically reacting horizontal plate in a porous media. Math Probl Eng. 2014;2014:1–10. Available from: https://doi.org/10.1155/2014/239082

30. Abolbashari MH, Freidoonimehr N, Nazari F, Rashidi MM. Analytical modeling of entropy generation for casson Nano-fluid flow induced by a stretching surface. Adv Powder Technol. 2015;26(2):542–552. Available from: https://doi.org/10.1016/j.apt.2015.01.003

31. Hakeem AKA, Ganesh NV, Ganga B. Magnetic field effect on second order slip flow of nanofluid over a stretching/shrinking sheet with thermal radiation effect. J Magn Magn Mater. 2015;381:243–257. Available from: https://doi.org/10.1016/j.jmmm.2014.12.010

32. Khan RA, Ullah H, Raja MAZ, Khan MAR, Islam S, Shoaib M. Heat transfer between two porous parallel plates of steady nanofluids with Brownian and thermophoretic effects: a new stochastic numerical approach. Int Commun Heat Mass Transf. 2021;126:105436. Available from: https://doi.org/10.1016/j.icheatmasstransfer.2021.105436

33. Aljohani JL, Alaidarous ES, Raja MAZ, Shoaib M, Alhothuali MS. Intelligent computing through neural networks for numerical treatment of non-Newtonian wire coating analysis model. Sci Rep. 2021;11(1):9072. Available from: https://www.nature.com/articles/s41598-021-88499-8

34. Shah Z, Raja MAZ, Chu YM, Khan WA, Abbas SZ, Shoaib M, et al. Computational intelligence of Levenberg-Marquardt backpropagation neural networks to study the dynamics of expanding/contracting cylinder for cross magneto-nanofluid flow model. Phys Scr. 2021;96(5):055219. Available from: http://dx.doi.org/10.1088/1402-4896/abe068

35. Ganesh NV, Hakeem AKA, Ganga B. A comparative theoretical study on Al$_2$O$_3$ and γ-Al$_2$O$_3$ nanoparticles with different base fluids over a stretching sheet. Adv Powder Technol. 2016;27(2):436–441. Available from: https://doi.org/10.1016/j.apt.2016.01.015

36. Abbas I, Hasnain S, Alatawi NA, Saqib M, Mashat DS. Thermal radiation energy performance on stagnation-point flow in the presence of base fluids ethylene glycol and water over stretching sheet with slip boundary condition. Energies. 2022;15(21):7965. Available from: https://doi.org/10.3390/en15217965

Citation: Abbas I. Analysis and Modeling of Heat and Mass Transfer in Alumina-water Nanofluids using Levenberg-Marquardt Backpropagation Neural Networks (LMT-ABPNN). Ann Math Phys. 2025;8(2):060-070. Available from: https://dx.doi.org/10.17352/amp.000147